

Smooth Reverse Subdivision

Javad Sadeghi*, Faramarz F. Samavati

Department of Computer Science, University of Calgary, Alberta, Canada

Abstract

In this paper we present a new multiresolution framework that takes into consideration reducing the coarse points' energy during decomposition. We start from initial biorthogonal filters to include energy minimization in multiresolution. Decomposition and reconstruction are main operations for any multiresolution representation. We formulate decomposition as smooth reverse subdivision, based on a least squares problem. Both approximation of overall shape and energy are taken into account in the least squares formulation through different weights.

Using this method, significant smoothness in decomposition of curves and tensor product surfaces can be achieved; while their overall shape is preserved. Having smooth coarse points yields details with maximum characteristics. Our method works well with synthesizing applications in which re-using high energy details is important. We use our method for finding the smooth reverse of three common subdivision schemes. We also provide examples of our method in curve synthesis and terrain synthesis applications.

Key words: multiresolution, reverse subdivision, energy minimization, least squares, wavelets

1. Introduction

Multiresolution is a hierarchical representation that allows decomposition of high resolution data to a lower resolution, in such a way that the original data can be reconstructed exactly. To do this efficiently, we need a convenient way to store error information compactly. This error information is usually accounted by a linear combination of functions known as wavelets. Multiresolution encapsulates two processes: decomposition (reverse subdivision plus error representation), and reconstruction (subdivision plus error correction). These processes can be performed using local filters obtained from rows or columns of banded matrices.

In general, high resolution data points may not represent the result of a subdivision scheme. The difference between fine points and subdivided coarse points is a residual vector which represents the error created when reversing subdivision. This vector contains high-frequency information or the noise of original fine points. Since the key characteristics of models (e.g. bumpiness of terrains) belong to high frequency parts of them, which are captured as detail vectors during decomposition, we can consider details as representatives of these characteristics.

In many applications the high energy characteristics captured as details are re-used for generating more realistic results. For example, in terrain synthesis by example <2>, details of a high-resolution terrain are extracted and then applied to a low-resolution base terrain. In this way a new terrain (with overall structure of the base terrain) can be synthesized with the same

small level characteristics of the example high-resolution terrain. The important role of details in example-based applications motivated us to examine whether current multiresolution techniques create details with the best quality. A related question is: in general, what conditions should be considered to find details that better approximate the characteristics of real objects and can be used properly for synthesizing detailed objects?

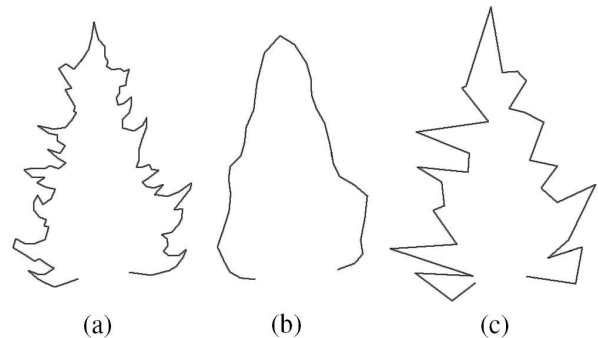


Figure 1: (a) Original silhouette curve. (b) Smooth reverse subdivision. (c) Cubic B-spline reverse subdivision.

As pointed out in <4>, multiresolution approach for synthesizing objects does not work properly when base model (low resolution) is noisy. The multiresolution approach requires that all characteristic information reside in the high-frequencies of the model, and all *sweep* information in the low-resolution of the target shape. Therefore, it is necessary to use a multiresolution scheme that creates a low-resolution model with minimum energy. To have a better understanding of this issue, consider decomposition of the fine curve in Figure 1(a) using two different multiresolution filters. The first method creates a smooth

*Corresponding author

Email addresses: jsadeghi@ucalgary.ca (Javad Sadeghi), samavati@ucalgary.ca (Faramarz F. Samavati)

coarse curve as shown in Figure 1(b), but the second method ends up to a harsh coarse curve as Figure 1(c).

When the coarse points are not smooth (Figure 1(c)) some extra information regarding the geometry is also stored in the details. This is not high-energy information, but is necessary to compensate extra deviations of coarse points. However, in Figure 1(b) because of the smoothness of the coarse curve the details more closely represent the high frequency characteristics of the object.

Currently, energy minimization for the low-resolution model has not been enforced in the construction of subdivision-based multiresolution representations. Possibly this is due to the presence of the energy term that makes derivation of a full set of multiresolution filters complicated. This paper contributes a novel method for multiresolution based on reversing subdivision with energy minimization of the low-resolution model. We introduce a new approach to obtain the necessary multiresolution operations from initial biorthogonal filters such as reverse subdivision <8> and constrained wavelets <5> filters. We also demonstrate the effectiveness of our method through example applications in curve and surface synthesis. In the curve example, by extracting the low-level details of hand-drawn strokes, more realistic synthetic strokes are created. Similarly, by applying a more natural characteristic resulting from smooth reverse subdivision to a base smooth terrain, a high-resolution realistic synthesized terrain is created.

This paper is organized as follows: Section 2 provides necessary background information. Section 3 presents details of the technique used to derive a new set of reverse subdivision filters. Section 4 demonstrates our approach with several multiresolution example schemes. Section 5 demonstrates some example applications of our method. Section 6 provides some evaluations and discussions. Finally, section 7 concludes the paper and provides possible future directions.

2. Background and Related Works

In this section, we introduce basic notations and discuss related works. We adapt the notation of Finkelstein and Salesin <6> and Olsen et al. <5> for the rest of this paper.

2.1. Multiresolution and Reverse Subdivision

The multiresolution research to date has mostly focused on wavelets. Let C^n denote a set of discrete fine points defining an object. Using *analysis filter matrices* A^n and B^n we can decompose C^n to a set of coarse points C^{n-1}

$$C^{n-1} = A^n C^n \quad (1)$$

and a high frequency set of details D^{n-1}

$$D^{n-1} = B^n C^n. \quad (2)$$

This process is known as *decomposition*. Details contain the information missing in decomposition process which can be represented as wavelet coefficients. Together C^{n-1} and D^{n-1} are

used in the *reconstruction* process to restore C^n using *synthesis filter matrices* P^n and Q^n

$$C^n = P^n C^{n-1} + Q^n D^{n-1}. \quad (3)$$

C^n can be decomposed recursively to C^l , C^{l+1} , ..., C^{n-1} and details D^l , D^{l+1} , ..., D^{n-1} where $l < n$. The reconstruction sequence of C^l , D^l , D^{l+1} , ..., D^{n-1} is known as a *wavelet transform*. The minimum condition of a biorthogonal multiresolution system is:

$$\begin{bmatrix} A \\ B \end{bmatrix} [P|Q] = \begin{bmatrix} I & 0 \\ 0 & I \end{bmatrix} = I \quad (4)$$

which implies the reconstruction process is the inverse of the decomposition process¹.

Samavati and Bartels <7> pioneered a reverse subdivision approach for constructing multiresolution representation. For a given subdivision scheme P and a set of fine data C^n , the coarse data C^{n-1} is determined such that PC^{n-1} has a minimal distance from the original fine points C^n . This can be expressed as following *global* least squares model:

$$\min \|C^n - PC^{n-1}\|_2^2. \quad (5)$$

By solving this model, C^{n-1} and a compact representation for the residual matrices A , B and Q are derived.

Later Bartels and Samavati <8> applied the same idea to derive *local* reverse subdivision filters using local linear conditions (LLC).

Olsen et al. <5> introduced another framework of constructing multiresolution based on constrained wavelets. This approach utilizes the relation between odd and even rules of subdivision filters to construct an efficient data structure for multiresolution.

Multiresolution representation has been used in various curve and surface applications. Finkelstein and Salesin <6> describe a wavelet-based multiresolution method that can capture and re-use a curve style. They edit the overall sweep of a curve by editing a low-resolution version of the curve without changing the original details. Kobbelt and Schröder <25> present a multiresolution construction setting for variationally optimal, interpolating subdivision curves. They also build stable wavelet bases in the uniform setting available to any algorithm that exploits multiresolution representation. Hahmann et al. <23> present a multiresolution framework for area preserving deformation of curves in different levels of details. The area is expressed as a bilinear form of the coarse and detail coefficients. An optimization process maintains the area constraint through all levels of resolution. Sauvage et al. <24> extend this approach to compute the volume enclosed by a multiresolution mesh using a trilinear form. They preserve the volume constraint using a quadratic minimization process when the mesh is deformed through multiresolution decomposition. Amanti <11> proposes a wavelet based multi-level analysis approach

¹For the sake of simplicity we drop the superscripts of matrices.

to fair planar cubic B-spline curves. This approach is useful to find the curve segments that need to be smoothed.

Gleicher <10> adapts Finkelstein and Salesin’s multiresolution curve fitting concepts to motion paths. A path is a time-varying curve which defines the position of a character at a given time. This work factorizes a previously captured motion to a path and a residual, then replaces the path with a new path to synthesize a different motion. Foster et al. <12> use multiresolution to remove and filter artifacts and noises from silhouette chains. Mündermann et al. <13> use reverse subdivision filters to reduce the number of vertices of a digitized raw data of a leaf in their work on modeling lobed leaves. They then use these points as control points of a B-spline curve. Cherlin et al. <14> use reverse subdivision for finding an appropriate parametric representation for sketched strokes. These strokes are the output of a mouse or a digitized pen. Consequently they have many noisy points.

In some multiresolution applications details play more important role. Brunn et al. <15> present a mechanism for high-quality style extraction and re-application using reverse subdivision. They use both Chaikin and cubic B-spline multiresolution filters from <7> and <8> and in both cases can achieve good results without a noticeable difference. Brosz et al. <2> use similar approach to extract and re-use the high-frequency characteristics from a target terrain in their terrain synthesis by-example system. Wecker et al. <16> use multiresolution to fix the *voids* commonly found in digital elevation models. They first fill the void with a smooth patch. Then extract the low-scale characteristics from the surrounding area of the void and apply them to this smooth patch. In Wecker et al. <17> a reverse subdivision-based multiresolution is employed for synthesizing irises. They capture necessary characteristics from existing irises which are then combined to form new ones.

All of these works benefit from compact and elegant multiresolution representation. Even some of them have tried to involve surface and volume constraints in the multiresolution construction. However, these filters are not constructed such that guarantee all of the high-energy is contained in the details and all sweep information is in low resolution. For example, Brunn et al. <15> explicitly highlight importance of the smoothness of the base path to improve re-application of a style for curve synthesis by example: “If the base path is not smooth, too much detail is lost when the re-application replaces the base points, leading to a distorted style and sometimes unintuitive results”. Therefore, above-mentioned synthesizing applications have limitations when the target shapes are very different from the original shapes or when the base shapes are noisy <4>. On the other hand if we have a multiresolution framework providing a good approximation of the original data, as well as minimizing the coarse points’ energy; the quality of synthesizing applications will be increased dramatically.

2.2. Curve Energy

In our multiresolution framework we take into consideration minimization of the energy of the coarse points $C = [c_0, c_1, \dots, c_n]^T$. Therefore, we need to find a simple curve en-

ergy approximation. This is enough for tensor-product surfaces due to their regular structure.

Discrete differential operators play a central role in curve and surface applications such as model smoothing. Botsch et al. <18> define the *intrinsic* geometry of a curve as length or angles of lines between points on the curve. Since the osculating circle <19> at point $p = x(t)$ provides a good local approximation to the curve, the curvature of the curve at $x(t)$, is defined as the reciprocal of the radius of the circle:

$$\kappa(t) = \frac{\|T'(t)\|}{\|x'(t)\|}. \quad (6)$$

In this notation $T(t)$ is the unit tangent vector $T(t) = \frac{x'(t)}{\|x'(t)\|}$. Therefore, if the parameter is arc-length we have $T(s) = x'(s)$ and can conclude:

$$\kappa(s) = \|T'(s)\| = \|x''(s)\|. \quad (7)$$

Since we deal with only discrete point sets, a discrete approximation of $\kappa(t)$ is preferred. The difference between c_i and its next or former points gives a discrete approximation of the first derivative at c_i . We use the notation of v_i for this derivative as:

$$v_i = c_{i+1} - c_i. \quad (8)$$

Considering $v_{i-1} = c_i - c_{i-1}$ and $v_i = c_{i+1} - c_i$, we use discrete Laplacian <20> (Δc_i) as a simple approximation of the curvature at c_i :

$$\Delta c_i = v_i - v_{i-1} = c_{i+1} - 2c_i + c_{i-1}. \quad (9)$$

In this calculation, a neighborhood of three points is used to approximate the curvature. By considering a larger neighborhood a more accurate approximation can be found. However, this makes our construction harder. In addition, in multiresolution construction a small neighborhood of a coarser level corresponds to a larger neighborhood of finer levels. Therefore, we found it is sufficient to use the neighborhood of three points.

Equation 9 can be represented as a matrix for a periodic (closed) point set:

$$M = \begin{bmatrix} -2 & 1 & 0 & \dots & 1 \\ 1 & -2 & 1 & & \\ & \ddots & \ddots & \ddots & \\ & & 1 & -2 & 1 \\ 1 & \dots & 0 & 1 & -2 \end{bmatrix}. \quad (10)$$

Each row of the M matrix shows a first-order Laplacian. The advantage of this approximation is that resulting equations are linear, helping us to calculate curve energy in terms of linear equations and banded matrix operations. For non-periodic curves we should prevent wrapping in the first and the last rows. We address this issue by using boundary definitions $c_1 - c_0$ for the first points and $c_{n-1} - c_n$ for the last points. These vectors are one-sided discrete tangents in boundaries that are suitable

enough for our approximation. Including these boundary conditions a sample 5×5 matrix is:

$$M = \begin{bmatrix} -1 & 1 & 0 & 0 & 0 \\ 1 & -2 & 1 & 0 & 0 \\ 0 & 1 & -2 & 1 & 0 \\ 0 & 0 & 1 & -2 & 1 \\ 0 & 0 & 0 & 1 & -1 \end{bmatrix}. \quad (11)$$

Now we can use $\|MC\|$ for approximating energy of C . We will next examine how achieving smooth approximation of coarse data changes the multiresolution process.

3. Reverse Subdivision with Energy Minimization

In this section, details of the steps to construct our multiresolution framework are discussed. Our goal is to find optimal coarse points that satisfy Equation 5, as well as having minimal overall energy. As discussed in Section 1, minimization of coarse energy will improve the level of detail extracted during decomposition and will directly benefit by-example applications.

In our approach we extend the least-squares formulation of <7> by including an energy term:

$$E(C^{n-1}) = \omega \|PC^{n-1} - C^n\|_2^2 + (1 - \omega) \|MC^{n-1}\|_2^2 \quad (12)$$

where $0 \leq \omega \leq 1$ is a weight parameter to control the importance of the energy versus fitness. From this equation C^{n-1} can be determined such that the error function $E(C^{n-1})$ be minimized.

For simplifying the notation, it is convenient to only consider the current level of resolution denoted by F and one lower level of resolution denoted by C . Therefore, Equation 12 can be simplified to:

$$E(C) = \omega \|PC - F\|_2^2 + (1 - \omega) \|MC\|_2^2. \quad (13)$$

Notice that we need not only to solve Equation 13 for finding A , but also to find a compact representation of the resulting Q and B filters <7>. The solution of 13 is also solution to the normal equation of the above minimization problem:

$$(\omega P^T P + (1 - \omega) M^T M)C = \omega P^T F. \quad (14)$$

Since $C = AF$, solving normal equation 14 for C provides A as:

$$A = (\omega P^T P + (1 - \omega) M^T M)^{-1} \omega P^T. \quad (15)$$

The matrix A is usually full and for practical implementation, it is better to solve banded linear system in Equation 14 instead of explicit use of inverse in Equation 15. For applications and scenarios that only need reverse subdivision, A is enough. However, for many applications such as by-example and model synthesizing, it is necessary to have a complete decomposition and reconstruction that requires determination of Q and B .

In contrast to the proposed A in <7> (the pseudo inverse of P), in our construction, A has more complex structure and consequently it is harder to determine Q and B to maintain biorthogonality (Equation 4). Because of this reason, it was not clear for us how to modify the construction of Q and B in <7> for A in Equation 15. This challenge directed us to use a technique similar to constrained wavelets <5> to achieve smooth reverse subdivision. Constrained wavelets provides a good structure that has the potential of starting from a simple multiresolution scheme and refining it to achieve a goal that in our work is minimization of the coarse points' energy while reducing the reconstruction error.

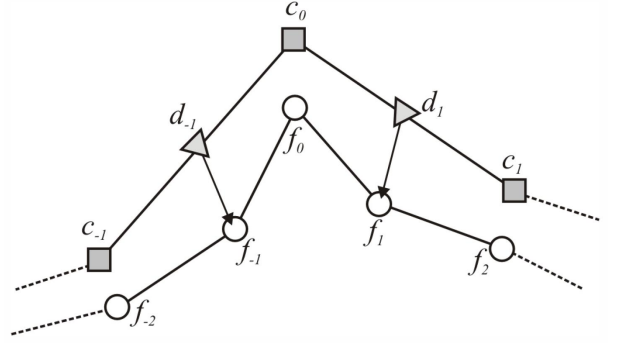


Figure 2: A fine curve F is decomposed to C , and odd fine points are replaced with their details. The even details can be computed from odd details.

As shown in Figure 2, starting from fine points denoted by f_i , a *trial* approximation of the coarse points denoted by c_i are stored at even vertices (in the fine level) and details denoted by d_i are stored at the odd vertices. For guaranteeing this structural property, it is necessary to enforce the following constraint (wavelet constraint): details at even vertices must be expressed as a linear combination of the details at neighboring odd vertices. As shown in <5>, based on this constraint, the decomposition and reconstruction matrices are determined. For example, the cubic B-spline subdivision matrix and corresponding banded trial matrices are as follows:

$$P = \begin{bmatrix} 1 & 0 & 0 & 0 & 0 & 0 & \dots \\ \frac{1}{2} & \frac{1}{2} & 0 & 0 & 0 & 0 & \dots \\ 0 & \frac{3}{4} & \frac{1}{4} & 0 & 0 & 0 & \dots \\ 0 & \frac{3}{16} & \frac{11}{16} & \frac{1}{8} & 0 & 0 & \dots \\ 0 & 0 & \frac{1}{2} & \frac{3}{4} & 0 & 0 & \dots \\ 0 & 0 & \frac{1}{8} & \frac{3}{4} & \frac{1}{8} & 0 & \dots \\ \vdots & \vdots & \vdots & \vdots & \vdots & \vdots & \vdots \\ \dots & 0 & 0 & \frac{1}{8} & \frac{11}{16} & \frac{3}{16} & 0 \\ \dots & 0 & 0 & 0 & \frac{1}{4} & \frac{3}{4} & 0 \\ \dots & 0 & 0 & 0 & 0 & \frac{1}{2} & \frac{1}{2} \\ \dots & 0 & 0 & 0 & 0 & 0 & 1 \end{bmatrix} \quad (16)$$

$$\tilde{A} = \begin{bmatrix} 1 & 0 & 0 & 0 & 0 & 0 & \cdots \\ -1 & 2 & 0 & 0 & 0 & 0 & \cdots \\ 0 & \frac{-1}{2} & 2 & \frac{-1}{2} & 0 & 0 & \cdots \\ & & & \vdots & & & \\ \cdots & 0 & 0 & 0 & 0 & 2 & -1 \\ \cdots & 0 & 0 & 0 & 0 & 0 & 1 \end{bmatrix} \quad (17)$$

$$\tilde{B} = \begin{bmatrix} \frac{3}{4} & \frac{-3}{2} & \frac{9}{8} & \frac{-1}{2} & \frac{1}{8} & 0 & \cdots \\ \cdots & \frac{1}{4} & -1 & \frac{-1}{2} & -1 & \frac{1}{4} & \cdots \\ & & & \vdots & & & \\ \cdots & 0 & \frac{1}{8} & \frac{-1}{2} & \frac{9}{8} & \frac{-3}{2} & \frac{3}{4} \end{bmatrix} \quad (18)$$

$$\tilde{Q} = \begin{bmatrix} 0 & 0 & 0 & 0 & \cdots \\ 0 & 0 & 0 & 0 & \cdots \\ 1 & 0 & 0 & 0 & \cdots \\ \frac{1}{4} & \frac{1}{4} & 0 & 0 & \cdots \\ & & \vdots & & \\ 0 & 0 & 0 & 0 & \cdots \\ 0 & 0 & 0 & 0 & \cdots \end{bmatrix}. \quad (19)$$

Although enforcing the above constraint provides a good data structure, the resulting trial matrices \tilde{Q} , \tilde{A} and \tilde{B} do not necessarily produce a good approximation. Olsen et al., explored a local refinement approach to perturb trial coarse points $\tilde{C} = [\tilde{c}_0, \dots, \tilde{c}_n]^T$ with a set of partial refinement vectors $\Delta = [\delta_0, \dots, \delta_n]^T$ for improving the approximation. This process has an equivalent representation in terms of lifting scheme <21> which facilitates finding final A and Q matrices. Figure 3 shows how refined coarse points $C = \tilde{C} + \Delta$ and trial details \tilde{D} create a closed-form multiresolution framework.

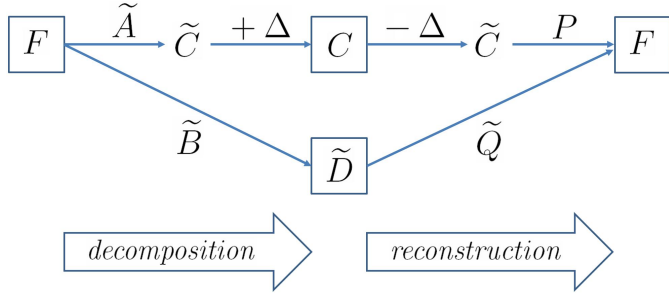


Figure 3: The constrained wavelets multiresolution framework.

Our main approach is to include refinement of the energy in this structure. However, if we consider discrete energy of coarse points in the same local refinement equations, it involves vertices out of the local neighborhood. This repetitively involves all of the vertices globally for the refinement process. Therefore, instead of perturbing coarse points one by one, we try to find the entire vector Δ globally to maintain interconnections between these points. To find the perturbation vector Δ we use perturbed $C = \tilde{C} + \Delta$ in the least squares formulation introduced in Equation 13:

$$E(\tilde{C} + \Delta) = \omega \|F - P(\tilde{C} + \Delta)\|_2^2 + (1 - \omega) \|M(\tilde{C} + \Delta)\|_2^2. \quad (20)$$

The normal equation of this general minimization problem is:

$$(\omega P^T P + (1 - \omega) M^T M)(\tilde{C} + \Delta) = \omega P^T F. \quad (21)$$

By replacing F with $P\tilde{C} + \tilde{Q}\tilde{D}$ in Equation 21 the normal equation can be written as:

$$(\omega P^T P + (1 - \omega) M^T M)\Delta = \omega P^T \tilde{Q}\tilde{D} - (1 - \omega) M^T M\tilde{C}. \quad (22)$$

We can find Δ from above linear system in linear time because $P^T P$, $M^T M$ and $P^T \tilde{Q}$ matrices have a banded structure. Then we can use Δ to find $C = \tilde{C} + \Delta$. Because of the minimization, the energy of new coarse points C and the distance of their subdivision to original fine points are reduced. It is not necessary to change \tilde{D} , \tilde{B} and \tilde{Q} because the trial matrices are consistent with the framework. We can find the final residual vector necessary to reconstruct the original fine points using the trial residual vector $F - PC = \tilde{Q}\tilde{D} - P\Delta$:

$$F - PC = F - P(\tilde{C} + \Delta) = \tilde{Q}\tilde{D} - P\Delta. \quad (23)$$

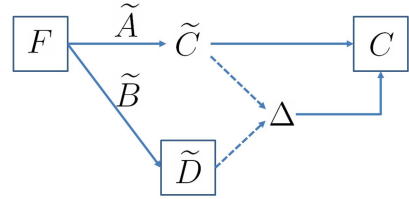


Figure 4: Our global decomposition process. Solid arrows denote the matrix multiplication while dotted arrows indicate the solution of a banded system.

As shown in Figure 4 the set of C and \tilde{D} finalize decomposition process of smooth reverse subdivision. Solid arrows denote a matrix operation (banded) while dotted arrows indicate the solution of linear system to find Δ . Algorithm 1 summarizes the decomposition process:

Algorithm 1 Smooth Reverse Subdivision

Input: $F, M, P, \tilde{Q}, \tilde{A}, \tilde{B}, \omega$

- 1: $\tilde{C} = \tilde{A}F$
- 2: $\tilde{D} = \tilde{B}F$
- 3: $\Delta = \text{Solution of the banded system (22)}$
- 4: $C = \tilde{C} + \Delta$

Output: C, \tilde{D}

For reconstruction of the original points using C and \tilde{D} , we use Equation 22. By replacing \tilde{C} with $C - \Delta$ we will achieve:

$$(\omega P^T P)\Delta = \omega P^T \tilde{Q}\tilde{D} - (1 - \omega) M^T M C. \quad (24)$$

Again Δ can be found in linear time operations because of the bandedness. Finally, we can calculate the residual vector from Equation 23 and add it to the subdivision of new coarse points to reconstruct F . Figure 5 and Algorithm 2, represent the process of reconstructing F from C and \tilde{D} . Again solid arrows

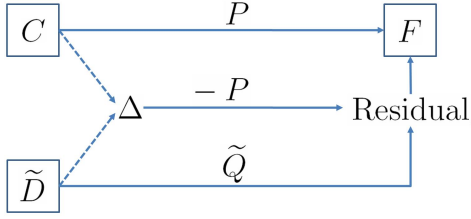


Figure 5: Our global reconstruction process. Solid arrows denote the matrix multiplication while dotted arrows indicate the solution of a banded system.

Algorithm 2 Reconstruction

Input: $C, \tilde{D}, M, P, \tilde{Q}, \omega$

- 1: $\Delta = \text{Solution of the banded system (24)}$
- 2: $\text{Residual} = \tilde{Q}\tilde{D} - P\Delta$
- 3: $F = PC + \text{Residual}$

Output: F

denote banded matrix operations and dotted arrows indicate the solution of a linear system.

Together, our decomposition and reconstruction processes form a multiresolution framework. Our approach utilizes least squares data fitting technique and discrete curve energy definition to find smooth coarse points that approximate the original fine points. Both decomposition and reconstruction operations cost linear time because of the bandedness of their matrix operations.

4. Example Schemes

Our approach is a natural fit for many subdivision schemes (curves and tensor product surfaces). To demonstrate our approach we have developed multiresolution settings for cubic B-spline, Dyn-Levin-Gregory <22> and quadratic B-spline.

4.1. Cubic B-spline

We start our approach from trial multiresolution matrices (Equations 16-19). We refer to the regular nonzero entries of these matrices as multiresolution filter. The P and \tilde{Q} matrices contain regular columns, each shifted downward by two elements from the previous column. Let \mathbf{p} and \mathbf{q} represent the non-zero entries of a regular column in P and \tilde{Q} respectively. Similarly, $\tilde{\mathbf{A}}$ and $\tilde{\mathbf{B}}$ are characterized by regular entries across the rows denoted by filters \mathbf{a} and \mathbf{b} , each shifted forward by two elements from the previous row. This notation helps us to compactly represent all involving trial filters. These filters for cubic B-spline multiresolution <5> are:

$$\begin{aligned}
 \mathbf{a} &= \begin{bmatrix} -\frac{1}{2} & 2 & -\frac{1}{2} \\ \frac{1}{4} & -1 & \frac{3}{2} & -1 & \frac{1}{4} \end{bmatrix} \\
 \mathbf{b} &= \begin{bmatrix} \frac{1}{8} & \frac{1}{2} & \frac{3}{4} & \frac{1}{2} & \frac{1}{8} \end{bmatrix} \\
 \mathbf{p} &= \begin{bmatrix} \frac{1}{4} & 1 & \frac{1}{4} \end{bmatrix} \\
 \mathbf{q} &= \begin{bmatrix} \frac{1}{4} & 1 & \frac{1}{4} \end{bmatrix}.
 \end{aligned} \tag{25}$$

For closed curves we can use these filters to create cyclic banded matrices with the same dimensions of the points on the curve.

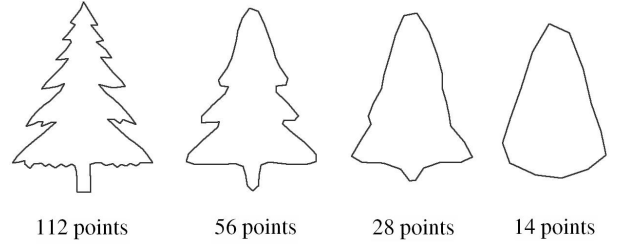


Figure 6: Results of recursive decomposition of a closed curve using our cubic B-spline approach.

There are some cases that the number of these fine points on the curve doesn't match exactly with the dimensions of resulting trial multiresolution matrices. For example, assume we want to decompose a periodic curve with 107 points three times. In this case we first *resample* the fine points to the next closest possible dimension (112 points). To do that we use fine points as control vertices of a cubic B-spline that creates the desired number of points. Then we can use the points of the resulting curve as our fine points. Because the resulting matrices have rows/columns that wrap around, they lose the structure of pure banded matrices. However, using the methods described in <7> we can still have linear time decomposition and reconstruction.

In our approach, a desired weighting should also be chosen to balance between smoothness of the coarse points and approximation of the fine points. If we have a noisy data, it is better to involve the energy term more, which means using smaller ω and if we have a smoother data, we can use larger ω . Notice that using a large energy term (a small ω) may reduce the effect of multi-scale property in multiresolution representation (it is usually expected that the scale of details in higher resolution be smaller than low resolution ones).

Figure 6 shows a closed curve representing a tree profile with three levels of smooth reverse subdivision. As shown, the curve has lost its deviations during different levels of decomposition.

For open curves (with boundaries) we use the same trial matrices of constrained wavelets <5> in Equations 16, 17, 18 and 19. This will help us to compare the performance of our approach with the constrained wavelets later. In general, our approach can be easily extended to tensor-product surfaces (e.g. terrain). These kinds of surfaces can be represented by two classes of curves usually denoted by u- and v-curves. Therefore, we can employ curve multiresolution for them. We can resample an open curve using the same method discussed for closed curves. Since we have two dimensional grid of elevations in a terrain, we should re-parameterize it in both dimensions.

Figure 7 shows a real terrain from Kansas, USA <1> with three levels of decomposition. As illustrated, we have achieved smooth low-resolution terrains with the overall structure of the original high-resolution terrain.

4.2. Dyn-Levin-Gregory

Dyn et al. <22> describe an interpolating subdivision scheme based on a four-point filter for odd points. Since even

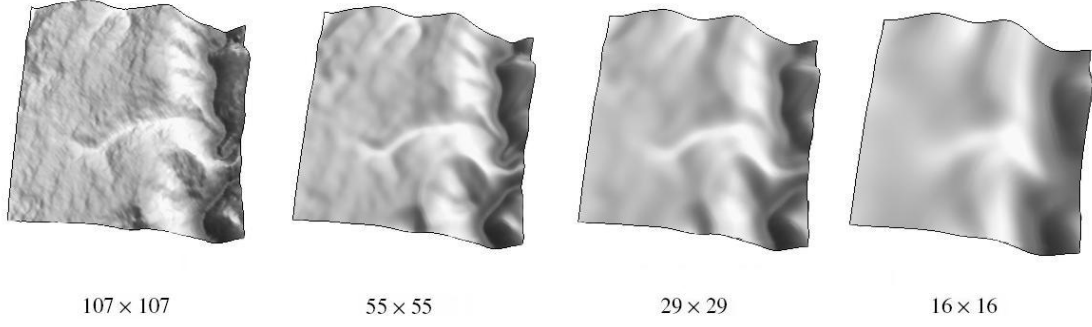


Figure 7: Results of recursive decomposition of a terrain using our cubic B-spline approach (with boundary).

points are not displaced by subdivision (they are interpolated), the trial filters are trivially defined as:

$$\begin{aligned}
 \mathbf{a} &= \begin{bmatrix} 0 & 1 & 0 \end{bmatrix} \\
 \mathbf{b} &= \begin{bmatrix} \frac{1}{16} & 0 & -\frac{9}{16} & 1 & -\frac{9}{16} & 0 & \frac{1}{16} \end{bmatrix} \\
 \mathbf{p} &= \begin{bmatrix} -\frac{1}{16} & 0 & \frac{9}{16} & 1 & \frac{9}{16} & 0 & -\frac{1}{16} \end{bmatrix} \\
 \mathbf{q} &= \begin{bmatrix} 0 & 1 & 0 \end{bmatrix}.
 \end{aligned} \tag{26}$$

We use these filters to construct trial multiresolution matrices with the same dimensions of the curve points and resample the fine points if necessary using the approach discussed in Section 4.1. Then we can construct the normal Equations 22 and 24 with resulting trial matrices for Dyn-Levin-Gregory four-point subdivision. Finally, we use the result in our proposed Algorithm 1 and 2 to implement smooth reverse subdivision and reconstruction based on a given weight. Figure 8 shows a closed curve with three levels of smooth reverse subdivision using our four-point approach.

In Figure 9 we visualize the residual vectors resulting from smooth reverse subdivision. Figure 9(a) shows profile of a face with 96 points. This curve is decomposed twice using our four-point approach to get a smooth coarse approximation. The red curve in Figure 9(b) shows the result of subdividing the coarse points two times without considering residual vectors that are shown with blue lines.

4.3. Quadratic B-spline

Our approach is capable of starting from any initial biorthogonal multiresolution. Here we start our construction using the following trial subdivision filters of quadratic B-spline (commonly referred to as Chaikin subdivision) <3>:

$$\begin{aligned}
 \mathbf{a} &= \begin{bmatrix} -\frac{1}{4} & \frac{3}{4} & \frac{3}{4} & -\frac{1}{4} \end{bmatrix} \\
 \mathbf{b} &= \begin{bmatrix} \frac{1}{4} & -\frac{3}{4} & \frac{3}{4} & -\frac{1}{4} \end{bmatrix} \\
 \mathbf{p} &= \begin{bmatrix} \frac{1}{4} & \frac{3}{4} & \frac{3}{4} & \frac{1}{4} \end{bmatrix} \\
 \mathbf{q} &= \begin{bmatrix} -\frac{1}{4} & -\frac{3}{4} & \frac{3}{4} & \frac{1}{4} \end{bmatrix}.
 \end{aligned} \tag{27}$$

We use these filters for our trial multiresolution matrices and if it is necessary use the same resampling technique discussed in Section 4.1. We can then enhance these initial multiresolution matrices to minimize the energy of coarse points while

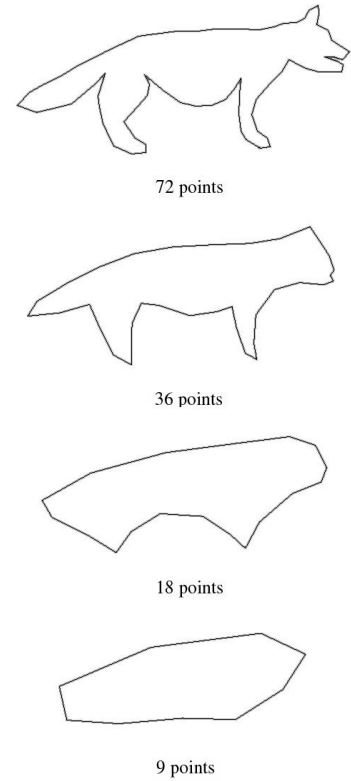


Figure 8: Results of recursive decomposition of a closed curve using our four-point interpolating approach.

reducing the reconstruction error using Algorithm 1 and 2. Figure 10 shows a closed curve with three levels of smooth reverse subdivision using our quadratic B-spline approach.

5. Results

In this section, we demonstrate examples of using our approach in synthesizing applications.

5.1. Curve Synthesis by Example

Figure 11 compares two methods for synthesizing a tree profile, Brunn et al.'s curve synthesis by-example <15> (first row)

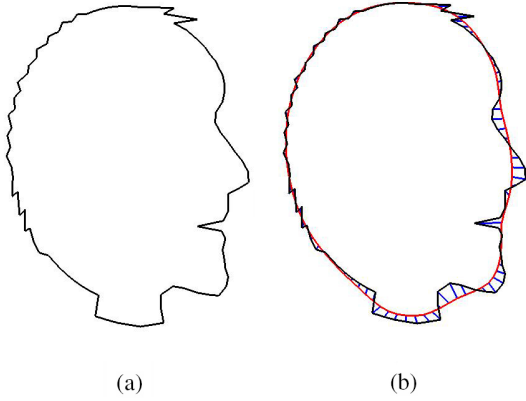


Figure 9: (a) A closed curve with 96 points. (b) Two levels of subdividing the coarse points resulting from two levels of four-point smooth reverse subdivision (the red curve) with corresponding residual vectors (the blue lines).

which is based on local multiresolution filters of $\langle 8 \rangle$ and our cubic B-spline approach (second row). For each row, column (a) shows the original data, column (b) shows its separation into two pieces to extract details as left and right half, column (c) shows a new smooth path that only contains large-scale variations and column (d) shows the result of applying silhouette styles of left and right profiles in (b) to coarse points in (c). As shown, in both cases a close approximation to the original tree is achieved. However, our approach shows noticeable improvement. It preserves exactly the same base paths of (c) which means our details just contain high-energy information without any extra deviation from overall sweep. This is particularly noticeable in the bottom-left and top-right portions of the tree's crown. Also, the bottom-left and top-left portions of the new crown show better arrangement of details, due to minimizing energy of the coarse points.

In this example we have used three levels of decomposition with $\omega = 0.72$ on an original fine curve with 179 points and the new base curve contains 25 points. When the number of new base coarse points is significantly less than the number of target fine points, we recursively subdivide the base points to achieve a larger number close to the number of target points. If a discrepancy remains, we use the same resampling technique described in Section 4.1 to equalize the number of the points. After achieving an equal number of points for both target and subdivided base points, we can decompose them up to any level with our smooth reverse subdivision filters. Then we can change the sweep of the target points at lower-resolution. This method of curve synthesis will face a problem when the orientation of details on the new curve are different from the target points. To address this issue, we use the same idea of Forsey and Bartels $\langle 9 \rangle$ which considers a local frame at the curve points as tangent to the curve and normal to the curve. Then we extract the angles between residual vectors and tangents to the curves at the curve points for each multiresolution level during the decomposition. We then use these angle vectors to re-orient the residual vectors on the new base points.

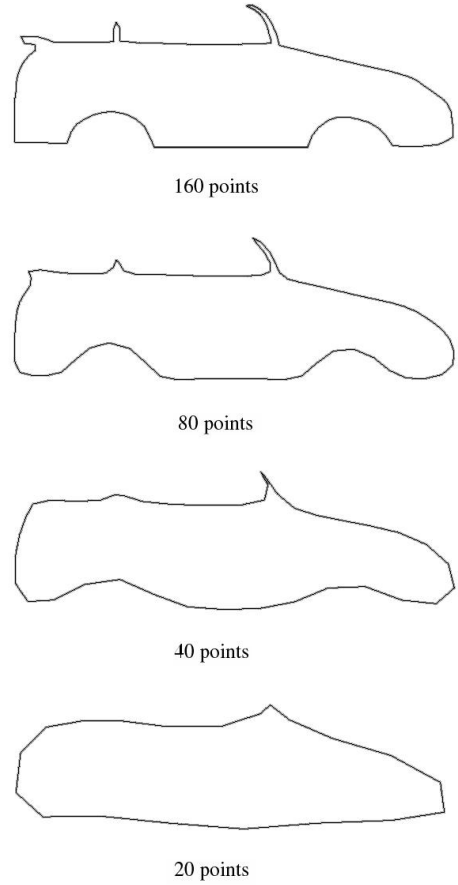


Figure 10: Results of recursive decomposition of a closed curve using our quadratic B-spline approach.

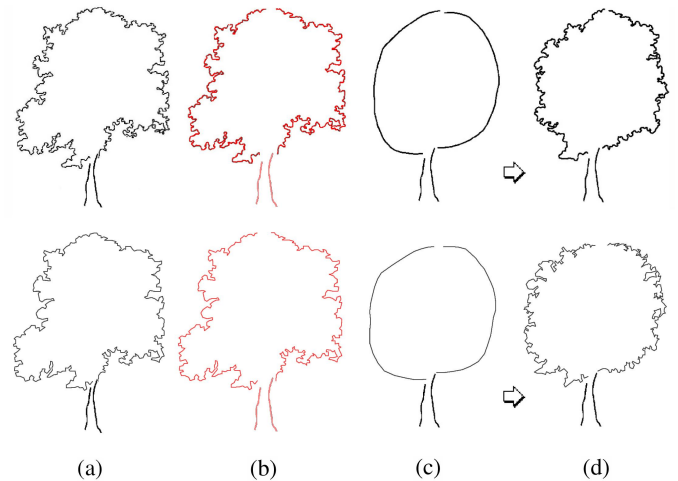


Figure 11: Extraction and re-application of tree silhouette styles using Brunn et al. (first row) and our cubic B-spline approach (second row). (a) Original illustration. (b) Extracted silhouette style in two parts. (c) A new smooth path. (d) Result of style re-application.

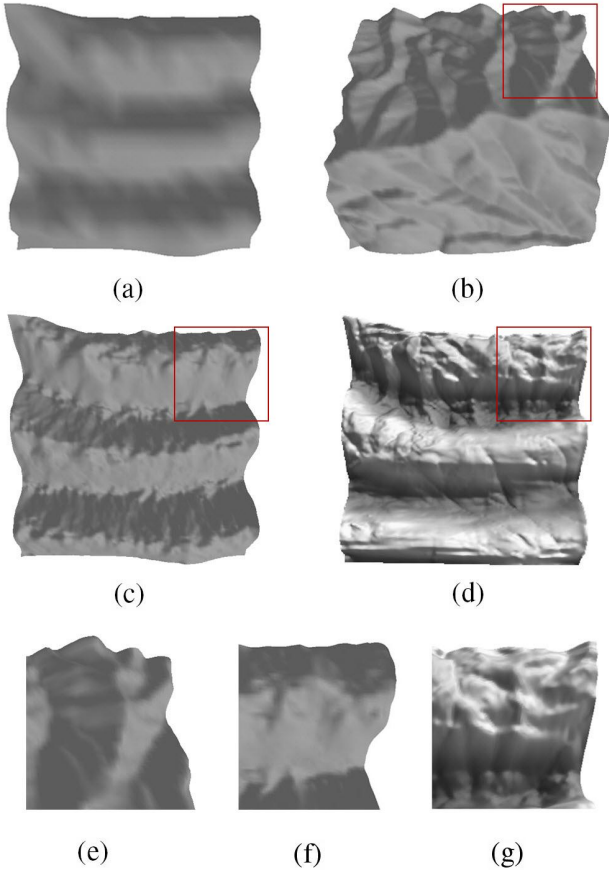


Figure 12: (a) A user-created 20×20 base terrain. (b) A real 103×103 target terrain. Results of extraction and re-application of terrain style using (c) Brosz et al. and (d) our cubic B-spline approach. (e), (f) and (g) are close-ups of top-right corners in (b), (c) and (d) respectively.

5.2. Terrain Synthesis by Example

In Figure 12, (a) shows a low-resolution (20×20) hand-made base terrain and (b) shows a high-resolution (103×103) target terrain from Rocky Mountains in Utah, USA <1>. Figure 12(c) shows the result of Brosz et al.’s terrain synthesis by-example <2> and Figure 12(d) shows the result of our cubic B-spline approach. We have created close-ups from top-right corners of Figure 12(b),(c) and (d) in Figure 12(e), (f) and (g) respectively. As shown, our result has a more appealing appearance because it transfers the characteristics of the target terrain to the base terrain more thoroughly. It is also noticeable that the lower part in Figure 12(d) has less jaggedness or deviation than the higher part, exactly the same as Figure 12(b).

In our example, we decomposed both of the target and subdivided base terrains with $\omega = 0.72$ two times to achieve 28×28 terrains. Then reconstructed the final terrain by applying extracted details of the target terrain to the new base terrain.

6. Evaluation and Discussion

In this section, we evaluate our approach and discuss some of its aspects. Figure 13 shows results of decomposing Figure 9(a)

up to three levels using cubic B-spline and Dyn-Levin-Gregory filters. For each row of Figure 13, columns (a), (b) and (c) show first, second and third levels of decomposition respectively. The corresponding curve energy for each curve is also calculated. The first row results from our cubic B-spline filters, the second row results from our Dyn-Levin-Gregory filters, the third row results from constrained wavelets’ cubic B-spline filters <5> and the last row results from constrained wavelets’ Dyn-Levin-Gregory filters. It explicitly shows that coarse curves resulted from our filters have significantly less energy than coarse curves from constrained wavelets’ filters. Also the Dyn-Levin-Gregory filters show better result than cubic B-spline filters. In general, four-point subdivision has a reverse with less energy than reverse of cubic B-spline. The main reason for this is that cubic B-spline subdivision is smoother scheme and reduces variations of the points during the forward subdivision. The reverse subdivision compensates this by exaggerating the variations.

All of the decomposition, reconstruction and synthesizing operations are done in linear time because we only need to solve banded linear systems of equations. Since all of the matrices are narrow banded in our example schemes, they can be solved in real-time.

Our approach also supports semiorthogonal wavelets such as <6> and <7>. In this kind of multiresolution, P and Q are banded matrices and explicitly derived while A and B are full matrices. Therefore, in our construction we start with P and $\tilde{Q} = Q$ and find \tilde{C} and \tilde{D} using Algorithm 1 and 2. Since \tilde{A} and B are full matrices, we avoid multiplications of full matrices in steps 1 and 2 of Algorithm 1 by solving following banded systems:

$$\begin{aligned} (P^T P)\tilde{C} &= P^T F \\ (\tilde{Q}^T \tilde{Q})\tilde{D} &= \tilde{Q}^T (F - P\tilde{C}). \end{aligned}$$

Figure 14 shows the effect of changing weight parameter from 0.01 to 1 on the same face profile in Figure 9(a). All of the results are from a single level of decomposition using our cubic B-spline approach. It demonstrates that by increasing the weight of the energy term (reducing ω) the coarse becomes smoother. Finding an appropriate ω depends on the specific application and the type of the data and can be found in a trial and error approach. However, it is possible to estimate a plausible default value for ω as function of the noisiness of the data. As a preprocessing step we can first drop the energy term from our construction by setting $\omega = 1$. After finding C from Algorithm 1 (or equivalently finding C from the trial filters) we use $g = \frac{\|MC\|}{n}$ as a measure for noisiness of the data (n is the size of the data). Then ω can be set as a linear function of g .

7. Conclusions and Future Works

This work presents a full multiresolution representation based on reverse subdivision, which balances the goals of producing a good approximation of the original points and producing smooth coarse points. Our derivation follows a global least squares model to minimize the energy of the coarse points. Our construction uses a trial set of multiresolution filters similar to

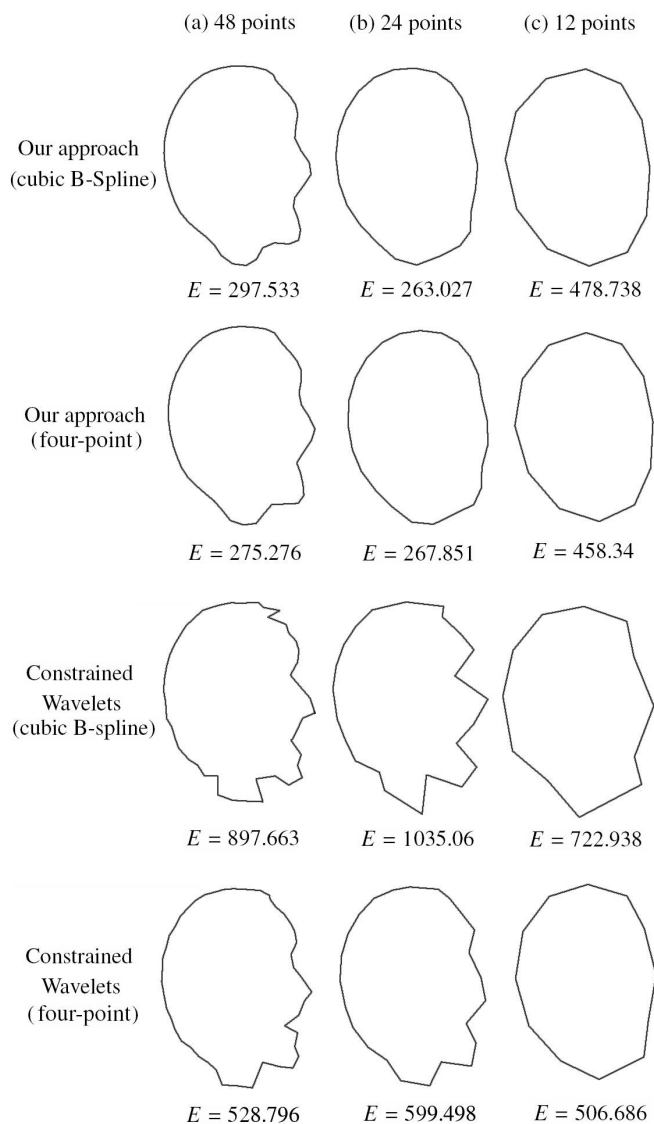


Figure 13: Three levels of decomposition of Figure 9(a) using our approach and constrained wavelets. The corresponding curve energy for each curve is represented.

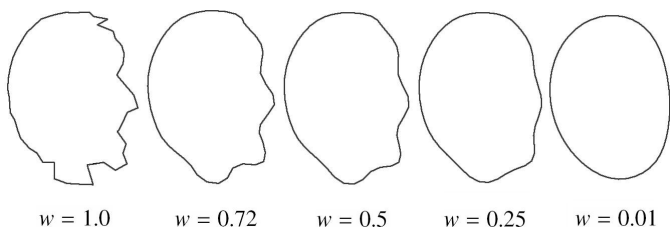


Figure 14: First level of decomposition of Figure 9(a) using our cubic B-spline approach with different weights.

the constrained wavelets framework. We provide a full set of operations for both decomposition and reconstruction. All operations in our technique are linear time due to the banded structure of matrices. It also gives freedom to the user to balance between smoothness and minimum error. To show the suitability of our method, we present different examples and also compare our approach with two recent curve synthesis and terrain synthesis applications.

Future work could include expanding our approach to find local A and B filters (currently, we solve banded linear systems instead of applying local filters). Using the local filters we can extend this approach to arbitrary topology surfaces. Our approach has also potential to generate interesting results in image compression. We also plan to use our filters in the area of motion synthesis to create animation by example. Finding the nature of the new lifting scheme underlying our technique is also an interesting future direction.

8. Acknowledgements

This work has been supported by the National Science and Engineering Research Council (NSERC) of Canada. The authors would like to thank Lakin Wecker for his contribution at the early stages of this research. We also wish to thank John Brosz and Luke Olsen for providing some of the examples and proof-reading the final manuscript.

References

- [1] USGS, Seamless data distribution system 2005, <http://seamless.usgs.gov>.
- [2] Brosz J, Samavati FF, Sousa MC. Terrain synthesis by-example. In: Braz J, Ranchordas A, Araújo H, Jorge J, editors. Communications in Computer and Information Science: Advances in Computer Graphics and Computer Vision 2008;4:58-77.
- [3] Samavati FF, Bartels RH, Olsen L. Local B-spline multiresolution with examples in iris synthesis and volumetric rendering. In: Yanushkevich S, Gavrilova M, Wang P, Srihari S, editors. Image Pattern Recognition: Synthesis and Analysis in Biometrics, Series in Machine Perception and Artificial Intelligence, World Scientific Publishing 2007;67(3):65-102.
- [4] Hertzmann A, Oliver N, Curless B, Seitz SM. Curve analogies. In: Proceedings of the 13th eurographics workshop on rendering, 2002.
- [5] Olsen L, Samavati FF, Bartels RH. Multiresolution for curves and surfaces based on constraining wavelets. Computers & Graphics 2007;31(3):449-62.
- [6] Finkelstein A, Salesin DH. Multiresolution curves. In: Proceedings of SIGGRAPH '94, 1994.
- [7] Samavati FF, Bartels RH. Multiresolution curve and surface representation: reversing subdivision rules by least-squares data fitting. Computer Graphics Forum 1999;18(2):97-119.
- [8] Bartels RH, Samavati FF. Reversing subdivision rules: Local linear conditions and observations on inner products. Journal of Computational and Applied Mathematics 200;119(1-2):29-67.
- [9] Forsey D, Bartels R. Hierarchical B-spline refinement. Computer Graphics 1988;22(4):205-12 [Proceedings of SIGGRAPH '88].
- [10] Gleicher M. Motion path editing. In: Proceedings of the 2001 symposium on interactive 3D graphics, 2001.
- [11] Amanti G. A multi-level filtering approach for fairing planar cubic B-spline curves. Computer Aided Geometric Design 2007;24(1):53-66.
- [12] Foster K, Sousa MC, Samavati FF, Wyvill B. Polygonal silhouette error correction: a reverse subdivision approach. International Journal of Computational Science and Engineering 2007;3(1):53-70.
- [13] Mündermann L, MacMurchy P, Pivovarov J, Prusinkiewicz P. Modeling lobed leaves. In: Proceedings of computer graphics international (CGI '03), 2003.

- [14] Cherlin JJ, Samavati F, Sousa MC, Jorge JA. Sketch-based modeling with few strokes. In: Proceedings of spring conference on computer graphics (SCCG '05), 2005.
- [15] Brunn M, Sousa MC, Samavati FF. Capturing and re-using artistic styles with reverse subdivision-based multiresolution methods. *International Journal of Images and Graphics* 2007;7(4):593-615.
- [16] Wecker L, Samavati F, Gavrilova M. Contextual void patching for digital elevation model. *The Visual Computer Journal* 2007;23(9-11):881-90.
- [17] Wecker L, Samavati F, Gavrilova M. Iris synthesis: a reverse subdivision application. In: Proceedings of GRAPHITE '05 conference, 2005.
- [18] Botsch M, Pauly M, Rossl C, Bischoff S, Kobbelt L. Geometric modeling based on triangle meshes. In: ACM SIGGRAPH 2006 courses, 2006.
- [19] Farin G, Sapidis N. Curvature and the fairness of curves and surfaces. *IEEE Computer Graphics and Applications* 1989;9(2):52-7.
- [20] Taubin G. A signal processing approach to fair surface design. In: Proceedings of the 22nd annual conference on computer graphics and interactive techniques, 1995.
- [21] Sweldens W. The lifting scheme: a construction of second generation wavelets. *SIAM Journal on Mathematical Analysis* 1997;29(2):511-46
- [22] Dyn N, Levine D, Gregory, J. A 4-point interpolatory subdivision scheme for curve design. *Computer Aided Geometric Design* 1987;4:257-68.
- [23] Hahmann S, Sauvage B, Bonneau GP. Area preserving deformation of multiresolution curves. *Computer Aided Geometric Design* 2005;22(4):349-67.
- [24] Sauvage B, Hahmann S, Bonneau GP. Volume preservation of multiresolution meshes. *Computer Graphics Forum* 2007;26(3):275-83.
- [25] Kobbelt L, Schröder P. A multiresolution framework for variational subdivision. *ACM Transactions on Graphics (TOG)* 1998;17(4):209-37.